SUPPORTING INFORMATION

Effects of Dioxygen Pressure on Rates of NO_x Selective Catalytic Reduction with NH_3 on Cu-CHA Zeolites

Casey B. Jones[1,†], Ishant Khurana[1,†], Siddarth H. Krishna[1], Arthur J. Shih[1], W. Nicholas Delgass[1], Jeffrey T. Miller[1], Fabio H. Ribeiro[1], William F. Schneider[2], Rajamani Gounder[1,*]

[1]*Charles D. Davidson School of Chemical Engineering, Purdue University, 480 Stadium Mall Drive, West Lafayette, IN 47907, USA*

[2]*Department of Chemical and Biomolecular Engineering, University of Notre Dame, 250 Nieuwland Science Hall, Notre Dame, IN 46556, USA*

[†]C. B. J. and I. K. contributed equally to this work.

*Corresponding author: rgounder@purdue.edu

Section S.1. Characterization data of H-CHA zeolite samples

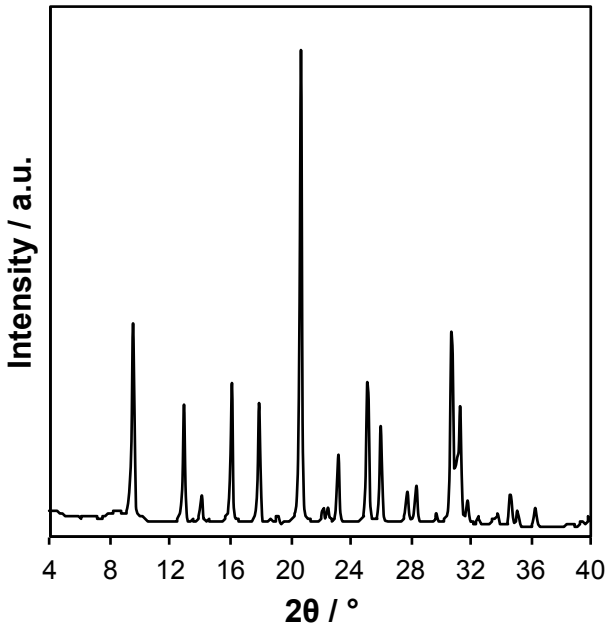

Figure S1. X-Ray diffraction pattern of a representative parent H-CHA (Si/Al = 15) sample prepared using methods reported in Paolucci et al. [1]

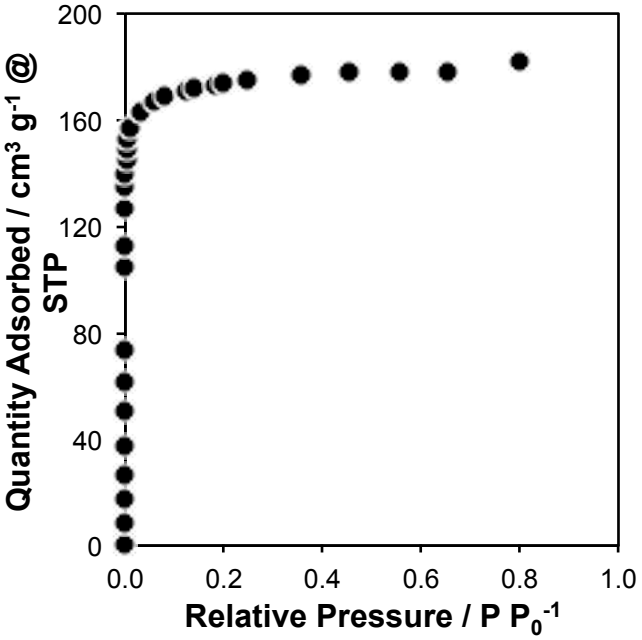

Figure S2. Ar adsorption isotherm (87 K) on a representative parent H-CHA (Si/Al = 15) sample prepared using methods reported in Paolucci et al. [1]

Section S.2. Characterization of Cu-CHA zeolites with varying Cu ion density

Cu-CHA samples with varying spatial density of isolated Cu sites (present either as Cu^{II} at paired framework Al or as $[Cu^{II}OH]^+$ at isolated framework Al) were studied here, as in our previous study [1]. These samples are denoted Cu-CHA-X, where X refers to the volumetric Cu density (atoms Cu per 1000 $Å^3$). Relevant structural and site characterization of these samples are provided in Table S1, including bulk elemental analysis, the number of Cu^{II} and $[Cu^{II}OH]^+$ sites (per Al), the concentration of Cu ions per crystallite volume, and the mean Cu-Cu distance. Additional Cu site characterization (*ex situ* X-ray absorption and UV-Visible spectra) can be found in our previous study [2].

Table S1. Characterization data of oxidized Cu^{II} forms of Cu-CHA-X samples (X = Cu volumetric density per 1000 $Å^3$). Elemental analysis, number of H^+ sites titrated by NH_3 on H-CHA and Cu-CHA samples, number of isolated Cu^{II} and $[Cu^{II}OH]^+$ sites, concentration of Cu ions per crystallite volume, and the mean Cu-Cu distance. Characterization data originally reported in our prior study [2].

Sample	Number of H^+ sites		Number of Cu sites			Cu / 1000 $Å^3$	Mean Cu-Cu distance (Å)
	H^+/Al (H-form)[a]	H^+/Al (Cu-form)	Cu/Al	Cu^{II}/Al*	$Cu^{II}OH$/Al*		
Cu-CHA-0.078	0.98	0.81	0.08	0.08	0.00	0.078	29.0
Cu-CHA-0.084	0.98	-	0.09	-	-	0.084	28.3
Cu-CHA-0.10	0.98	0.80	0.10	0.08	0.02	0.10	26.9
Cu-CHA-0.17	0.98	0.70	0.18	0.10	0.08	0.17	22.3
Cu-CHA-0.23	1.00	0.64	0.24	0.12	0.12	0.23	20.3
Cu-CHA-0.29	1.00	0.61	0.31	0.08	0.23	0.29	18.7
Cu-CHA-0.31	0.98	0.58	0.33	0.09	0.22	0.31	18.4
Cu-CHA-0.35	0.98	0.51	0.37	0.10	0.27	0.35	17.6

[a] Different parent samples of H-CHA (Si/Al = 15), from replicate syntheses, were used to prepare the Cu-form samples.

*Determined from a site balance considering total Cu/Al, the number of H^+ titrated on H-form and Cu-form samples, and the 2:1 and 1:1 H^+:Cu exchange stoichiometry expected for Cu^{II} and $Cu^{II}OH$, respectively.

Section S.3. Methods used to measure and calculate NO SCR rates by correcting for contributions of "fast" SCR reactions from NO_2

All reported NO SCR rates were corrected for contributions from the "fast" SCR reaction due to background NO_2, which is present as an impurity in NO cylinders and is formed by gas-phase NO oxidation. A blank reactor tube was loaded with 0.070 g SiO_2 to measure background NO_2 formation rates at fixed NO pressure (0.03 kPa) at 473 K, but with varying O_2 pressures (0.5–60 kPa O_2) and total gas flow rates (1.0–2.5 L min^{-1} at ambient temperature and pressure) (Fig. S3a). The gas-phase NO_2 concentration in the reactor outlet was linearly proportional to O_2 pressure (P_{O2}) and inversely proportional to gas flow rate F (i.e., proportional to gas residence time), with a constant of proportionality k, as shown in Figure S3a and as described by Equation (S1); the non-zero y-intercept b reflects NO_2 present as impurity levels in the NO cylinder.

$$[NO_2, background] = b + k(\frac{P_{O2}}{F})\,(\frac{P_{NO}}{0.03\ kPa\ NO})^2 \quad \text{(S1)}$$

NO_2 formation rates that show a first-order dependence on O_2 pressure and second-order dependence on NO pressure are consistent with gas-phase NO oxidation kinetics [3]. Background NO_2 formation rates indeed showed a nearly second-order dependence in NO pressure (0.015–0.060 kPa) (Fig. S3b). In order to correct for background NO_2 formation for experiments in which the NO pressure was varied from 0.03 kPa, such as when NO reaction orders were measured, Equation S1 also accounts for the second-order dependence of NO_2 formation rates on NO pressure. For these experiments, the y-intercept (b) of Figure S3a was also adjusted based on measurements of NO_2 concentration at 0 kPa O_2 and different NO pressures. Given that the background NO_2 concentration depends on the reactant source (e.g., NO_2 impurities in the NO cylinder) and reactor size and hydrodynamics (e.g., internal volumes of the reactor and gas lines, gas mixing patterns, gas residence time), the NO_2 background

concentration must be independently measured for each reactor system and NO cylinder used to measure SCR rates.

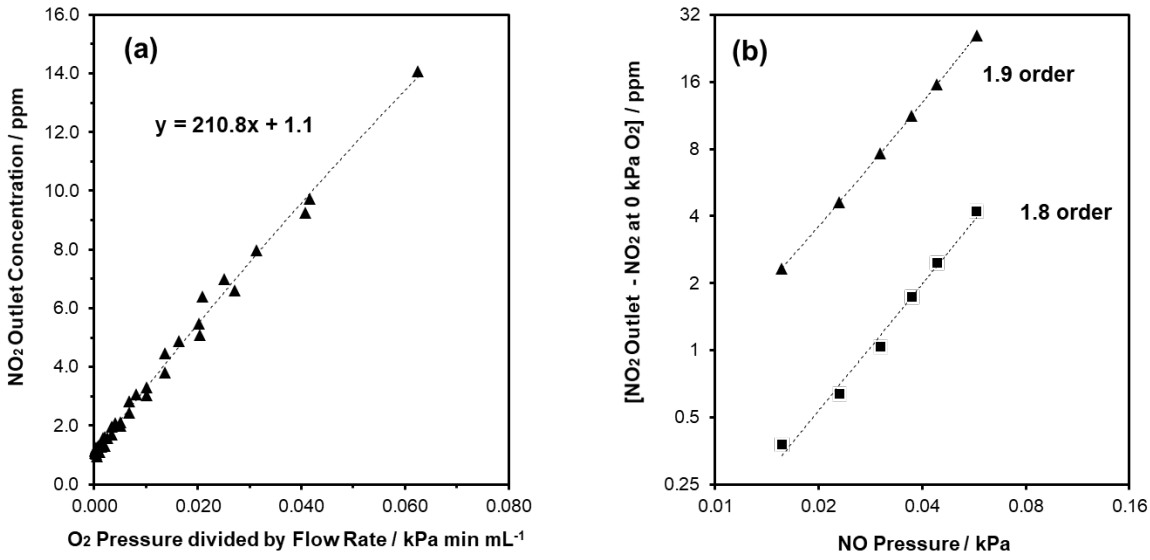

Figure S3. NO_2 concentration in reactor outlet of blank reactor experiments (SiO_2 only). (a) Variation of residence times and O_2 pressures. Dotted line represents regression of the data to Eq. (S1) (reaction conditions: 0.030 kPa NO, 0.030 kPa NH_3, 1–60 kPa O_2, 7 kPa CO_2, 1 kPa H_2O and balance N_2, 1.0–2.5 L min^{-1} total gas flow rate). (b) Variation of NO pressure. Linear fits were used to calculate NO reaction orders (reaction conditions: 0.015–0.060 kPa NO, 0.030 kPa NH_3, 10 (■) or 60 kPa (▲) O_2, 7 kPa CO_2, 1 kPa H_2O and balance N_2, 2.0 L min^{-1} total gas flow rate).

In experiments with Cu-CHA catalysts, the NO_2 consumed over the catalyst bed was calculated as the difference between NO_2 formed in the blank reactor and NO_2 measured in the outlet of the reactor in each experiment (Equation S2).

$$NO_2\ consumed\ = NO_2, background - NO_2, reactor\ outlet \quad \text{(S2)}$$

NO_2 consumption is assumed to occur through a "fast" SCR pathway, which consumes an equimolar amount of NO:

$$4\,NH_3 + 2\,NO + 2\,NO_2 \rightarrow 4\,N_2 + 6\,H_2O \quad \text{(S3)}$$

To calculate the rate of "standard" NO SCR, NO_2 consumption was subtracted from the total NO consumption:

$$NO_2\ consumed, standard\ SCR\ = NO\ consumed - NO_2\ consumed \quad \text{(S4)}$$

The ratio of "NO_2 consumed" to "NO consumed" is shown as a function of O_2 pressure for a representative sample (Cu-CHA-0.23) in Figure S4. For this sample, the magnitude of the "fast SCR correction" is 5-10% of the total NO consumption across all measured O_2 pressures.

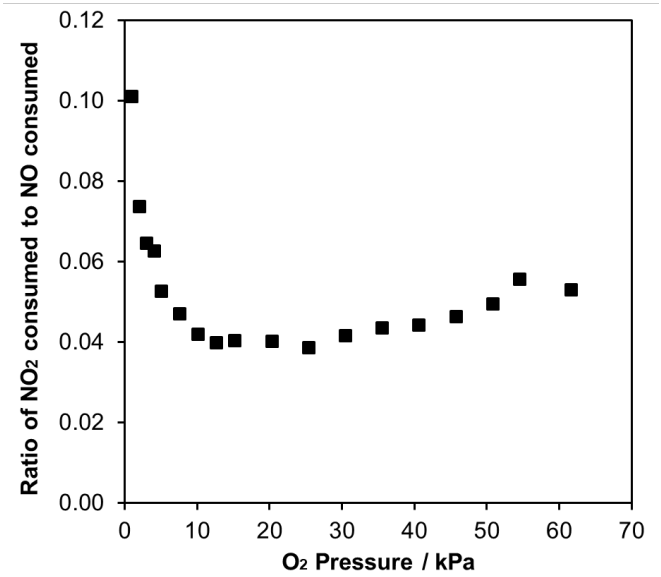

Figure S4. Ratio of "NO_2 consumed" to "NO consumed" as a function of O_2 pressure for Cu-CHA-0.23 (reaction conditions: 0.030 kPa NO, 0.030 kPa NH_3, 1–60 kPa O_2, 7 kPa CO_2, 1kPa H_2O and balance N_2).

For each Cu-CHA zeolite sample, SCR rates (473 K) at twenty O_2 pressures between 1–60 kPa were measured in random order, holding the concentration of other gases fixed (1 kPa H_2O, 7 kPa CO_2, 0.030 kPa NO, 0.030 kPa NH_3, balance N_2) while maintaining differential conversion. Figure S5 shows SCR rates as a function of varying O_2 pressure measured on Cu-CHA-0.23 in two different flow reactor systems of different internal volumes; the agreement between these measurements validates the methods described here to measure and calculate NO SCR rates.

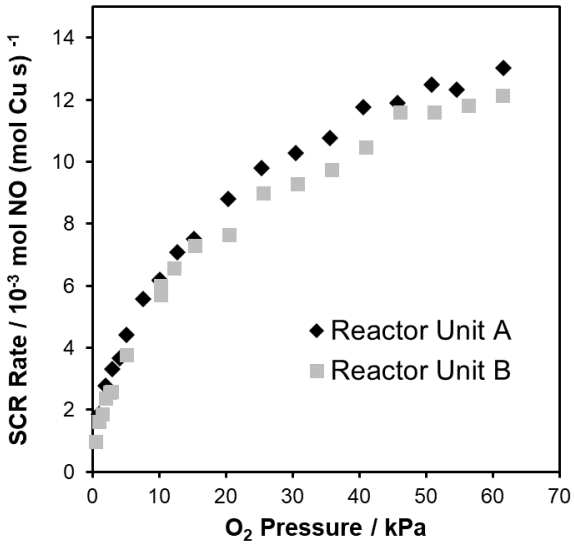

Figure S5. NO SCR rates (per Cu, 473 K) as a function of O_2 pressure in two separate reactor units for Cu-CHA-0.23 (reaction conditions: 0.030 kPa NO, 0.030 kPa NH_3, 1–60 kPa O_2, 7 kPa CO_2, 1 kPa H_2O and balance N_2). In order to account for background NO_2 formation in each reactor unit, the values of k and b in Equation S1 were measured independently for each system: Reactor Unit A (black diamonds), k = 210.9 (ppm mL min^{-1} kPa^{-1}); b = 0.73 ppm. Reactor Unit B (grey squares), k = 129.6 (ppm mL min^{-1} kPa^{-1}); b = 1.6 ppm.

Section S.4. Assessment of potential corruption of measured rates by transport phenomena

In order to assess the extent to which external transport phenomena influenced measured SCR rates, the gas hourly space velocity was varied from 1.13–2.26 (10^6 hr^{-1}) by varying total gas flow rates (1–2 L min^{-1} at ambient temperature and pressure) for Cu-CHA-0.084 at different O_2 pressures (1, 10, 30, and 60 kPa O_2). SCR rates were invariant with space velocity at all O_2 pressures (Figure S6), indicating that measured rates were uncorrupted by external transport processes, and confirming the absence of bed-scale gradients in concentration or temperature. The invariance of measured NO SCR rates with gas flow rate also shows that measured reaction rates are not influenced by changes to the gas-phase NO_2 concentration at the front of the catalyst bed.

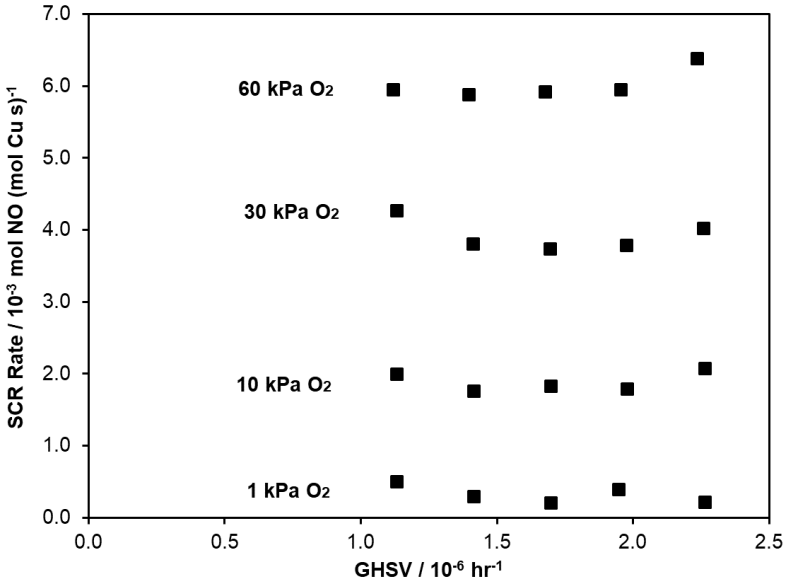

Figure S6. NO SCR rates (per Cu, 473 K) for Cu-CHA-0.084 as a function of gas hourly space velocity (reaction conditions: 0.030 kPa NO, 0.030 kPa NH_3, 1/10/30/60 kPa O_2, 7 kPa CO_2, 1 kPa H_2O and balance N_2).

The Weisz-Prater criterion (Equation S5) was used to estimate whether intracrystalline mass transport limitations affected measured rate data, and was calculated separately for O_2, NO, and NH_3, according to the following equation [4]:

$$N_{WP} = r_{obs}\, r_p^{\,2} / (C_s\, D_{eff}) \qquad \text{(S5)}$$

where r_{obs} is the reaction rate per volume, r_p is the crystallite radius and taken as half (0.75 μm) of the crystallite length (1.5 μm) measured from SEM images of H-form CHA zeolites reported in our prior study [5], and C_s is the reactant concentration at the crystallite surface and taken as the bulk fluid concentration in the absence of external transport limitations. The final parameter in Equation (S5) is D_{eff}, or the effective diffusivity of each molecule within zeolite crystallites, and were estimated according to:

(i) O_2: As an order-of-magnitude estimate, D_{eff} was taken as the diffusivity of O_2 in Zeolite 5A (LTA, containing 8-membered rings) at 303 K ($1.2* 10^{-7}$ m^2 s^{-1}) [6], scaled to the reaction temperature of 473 K using Chapman-Enskog theory (2.3×10^{-7} m^2 s^{-1}):

$$D_{eff,\,T2} = D_{eff,\,T1}\,(T_2/T_1)^{3/2} \quad \text{(S6)}$$

At the most severe condition (Cu-CHA-0.37, 1 kPa O_2), $N_{WP,O2} \sim 2 \times 10^{-5} << 1$, verifying the absence of significant intracrystalline O_2 transport limitations.

(ii) NO: The diffusivity of NO in LTA was not found in the literature; thus, as an order-of-magnitude estimate, D_{eff} was taken as the diffusivity of N_2 in Zeolite 5A (LTA, containing 8-membered rings) at 303 K ($6.8* 10^{-8}$ m^2 s^{-1}) [6], scaled to the reaction temperature of 473 K using Chapman-Enskog theory (1.3×10^{-7} m^2 s^{-1}) according to Equation (S6). At the most severe condition (Cu-CHA-0.37, 60 kPa O_2), $N_{WP,NO} \sim 6 \times 10^{-3} << 1$, verifying the absence of significant intracrystalline NO transport limitations.

(iii) NH_3: D_{eff} was set equal to the reported diffusivity of saturated NH_3 in Cu-CHA at 473 K ($1.2* 10^{-9}$ m^2 s^{-1}), which was measured using quasielastic neutron scattering on a 3 wt% Cu-CHA sample (Si/Al = 17) exposed to 80 kPa NH_3 [7]. $N_{WP,NH3}$ is plotted as a function of Cu density and O_2 pressure in Figure S7. $N_{WP,\,NH3} < 1$ at all conditions, suggesting the absence of

severe intracrystalline NH_3 transport limitations. These conservative estimates of $N_{WP,\ NH3}$ become > 0.1 at higher Cu densities and O_2 pressures, however, indicating that NH_3 diffusion might affect rates measured under certain conditions.

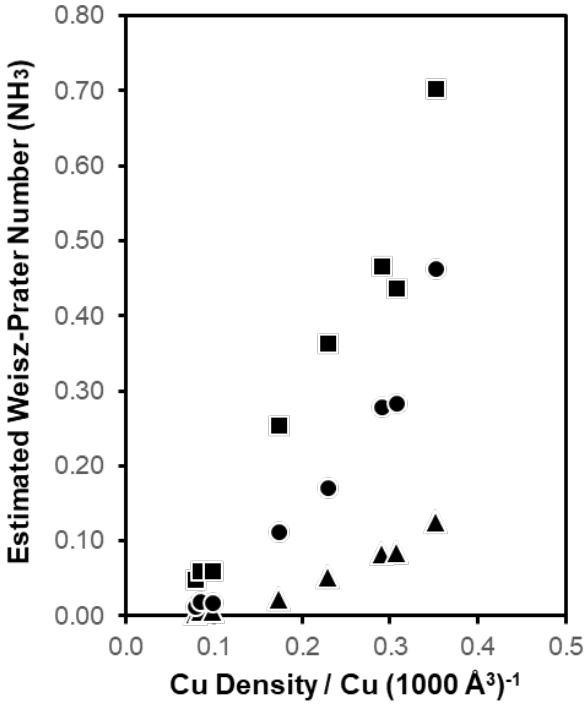

Figure S7. Estimated Weisz-Prater number for NH_3 as a function of O_2 pressure and Cu density for Cu-CHA-X samples. 1 kPa (triangles), 10 kPa (circles) and 60 kPa O_2 (squares) (reaction conditions: 0.030 kPa NO, 0.030 kPa NH_3, 1/10/60 kPa O_2, 7 kPa CO_2, 3 kPa H_2O and balance N_2 at 473 K).

Section S.5. Measurement of apparent reaction orders on Cu-CHA samples in low and high O_2 pressure limits

The data in Figure 2b (main text) are plotted in a log-log scale in Figure S8 to better visualize the quality of the fit between the measured data and the rate model (Eq. (3)).

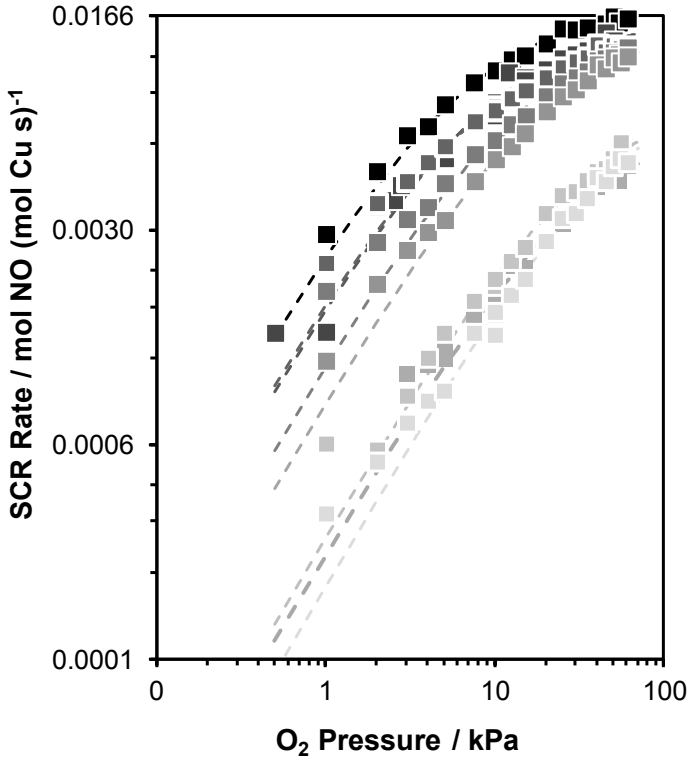

Figure S8. Steady-state SCR rates (per Cu) as a function of O_2 pressure plotted using logarithmic scales on Cu-CHA-X samples (light-to-dark shading as X increases). Dashed lines represent regression of the data to Eq. (3).

With increasing O_2 pressure (1–60 kPa), apparent NO orders increase systematically from 0.2 to 0.8, while apparent NH_3 orders remain essentially invariant near a value of -0.5 (Table S2).

Table S2. SCR kinetic parameters measured on Cu-CHA samples at 1, 10, and 60 kPa O_2.

Sample	1 kPa O_2		10 kPa O_2		60 kPa O_2	
	NO order[a]	*NH_3 order*[b]	*NO order*[a]	*NH_3 order*[b]	*NO order*[a]	*NH_3 order*[b]
Cu-CHA-0.078	-	-	0.4	-0.5	0.8	-0.5
Cu-CHA-0.17	0.3	-0.7	0.4	-0.5	0.7	-0.5
Cu-CHA-0.29	0.2	-0.5	0.6	-0.4	0.6	-0.4

[a] Other reaction conditions: 0.030 kPa NH_3, 7 kPa CO_2, 1 kPa H_2O and balance N_2 at 473 K
[b] Other reaction conditions: 0.030 kPa NO, 7 kPa CO_2, 1 kPa H_2O and balance N_2 at 473 K
Uncertainties are ± 0.1.

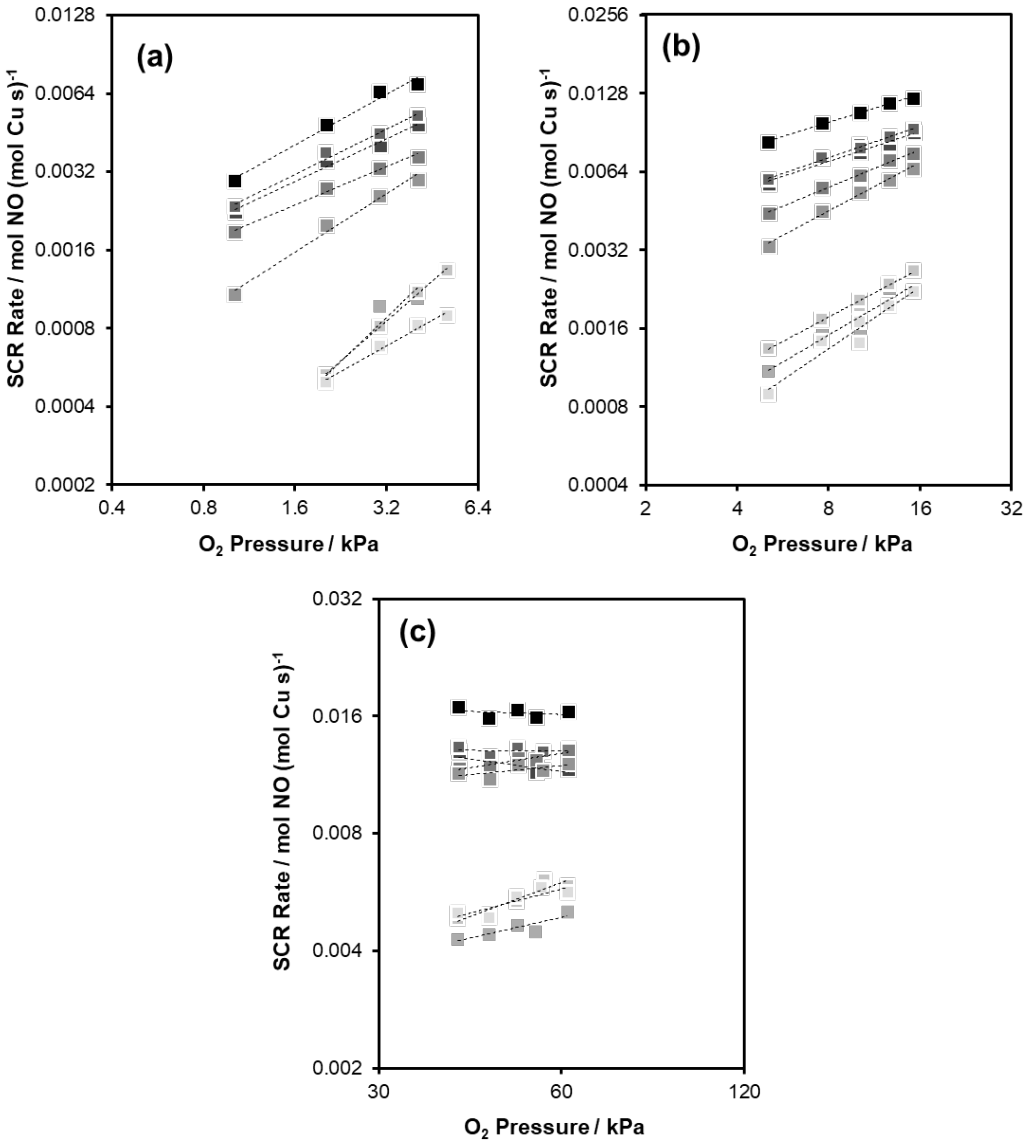

Figure S9. Steady-state SCR rate (per Cu) versus O_2 pressure on Cu-CHA-X samples (light-to-dark shading as X increases), along with best fit lines representing O_2 reaction orders, in the pressure ranges of (a) 1–4 kPa O_2 , (b) 5–15 kPa O_2, and (c) 40–60 kPa O_2. For Cu-CHA-0.78, Cu-CHA-0.084, and Cu-CHA-0.10, the O_2 reaction order in the low O_2 pressure range was instead reported from 2-5 kPa O_2 improve experimental accuracy, due to the low (~1%) NO conversion at 1 kPa O_2 for these samples.

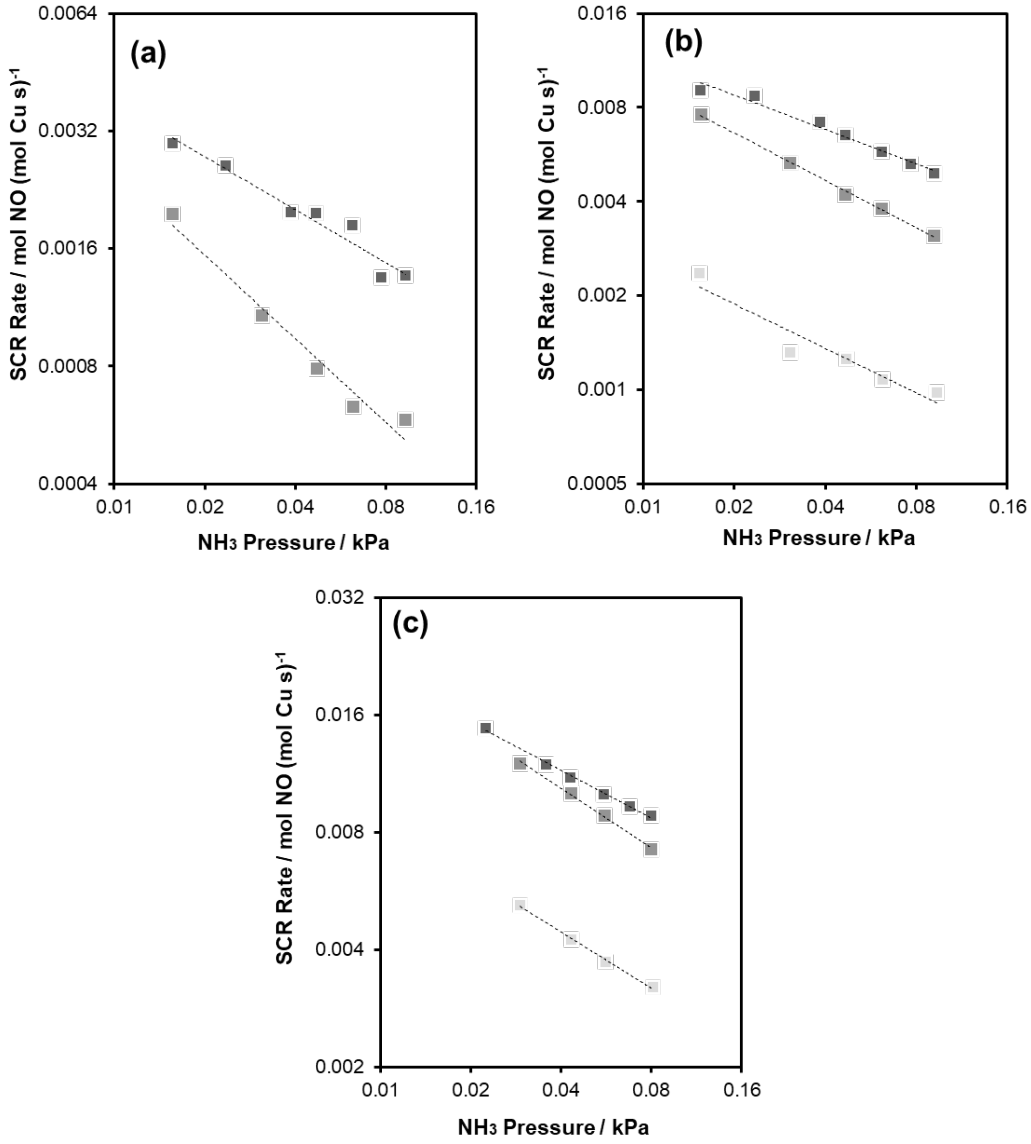

Figure S10. Steady-state SCR rate (per Cu) versus NH_3 pressure on Cu-CHA-0.078, Cu-CHA-0.17, and Cu-CHA-0.29 (light-to-dark shading as X increases), along with best fit lines representing NH_3 reaction orders, at various O_2 pressures: (a) 1 kPa O_2 (Cu-CHA-0.078 was omitted due to noisier measurements in this case), (b) 10 kPa O_2, (c) 60 kPa O_2.

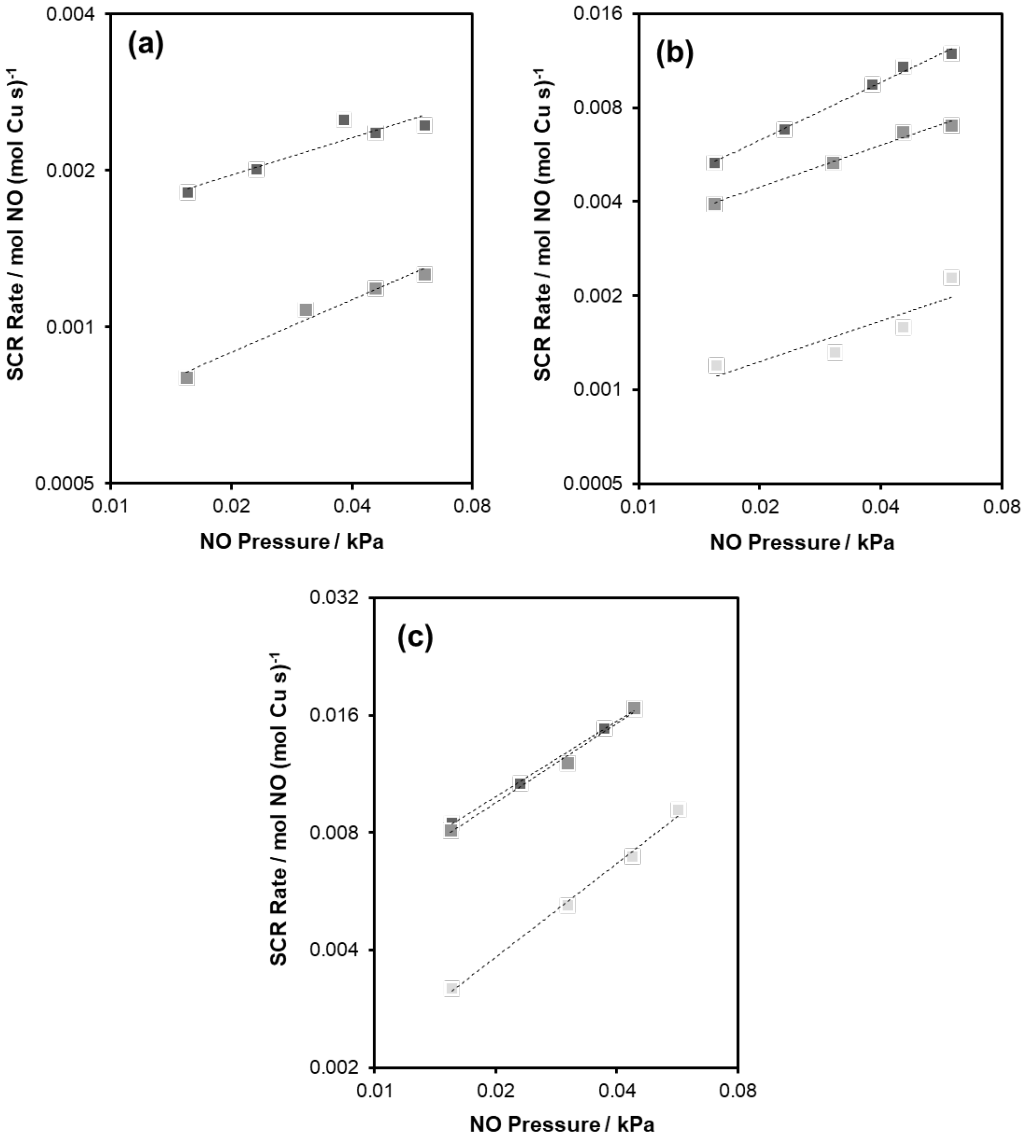

Figure S11. Steady-state SCR rate (per Cu) versus NO pressure on Cu-CHA-0.078, Cu-CHA-0.17, and Cu-CHA-0.29 (light-to-dark shading as X increases), along with best fit lines representing NO reaction orders, at various O_2 pressures: a) 1 kPa O_2 (Cu-CHA-0.078 was omitted due to noisier measurements in this case), b) 10 kPa O_2, c) 60 kPa O_2.

Section S.6. *In operando* XANES spectra of Cu-CHA-0.23 with varying O_2 pressure

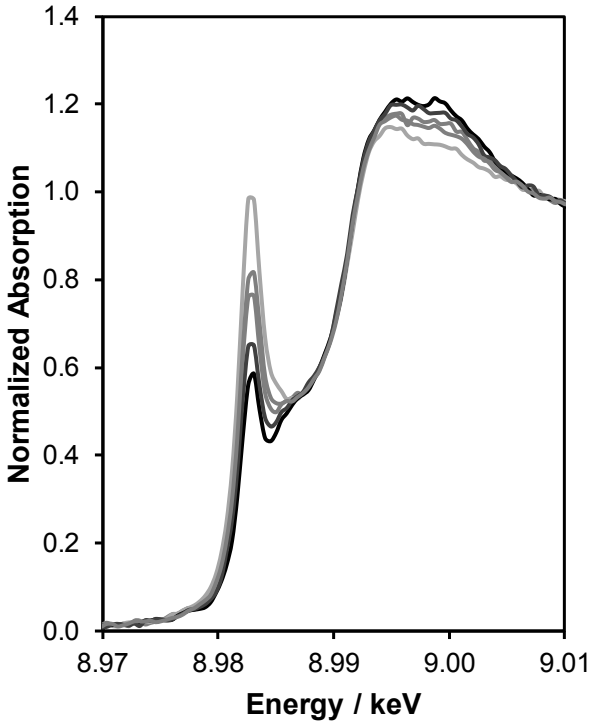

Figure S12. *In-operando* XANES spectra measured at 1 kPa O_2 5 kPa O_2, 10 kPa O_2, 30 kPa O_2, and 60 kPa O_2 (light to dark with increasing O_2 pressure). The balance gas compositions were 0.030 kPa NH_3, 0.030 kPa NO, 2 kPa H_2O, 7 kPa CO_2, and balance N_2. Linear combination fitting to Cu(I) and Cu(II) standards was performed as previously reported [1].

Section S.7. Transient O_2-assisted oxidation of pre-reduced Cu-CHA-X samples: Models to fit rate data and corresponding XANES spectra

As described in our previous study [2], the transient decrease of Cu^I with time (Fig. 4, main text) is best described by the following rate law, assuming an integral power on $[Cu^I]$:

$$\frac{d[Cu^I(t)]}{dt} = -2k_{ox}[Cu^I(t)]^2 \quad \text{(S7)}$$

In order to account for the unoxidizable Cu^I fraction (denoted as $[Cu^I(\infty)]$) observed in XANES spectra at the end of the transient O_2-assisted oxidation experiments (Figs. S13-S19), we define the concentration of Cu^I that can participate in the oxidation reaction as:

$$[Cu^I(t)]_{corr} = [Cu^I(t)] - [Cu^I(\infty)] \quad \text{(S8)}$$

$$\frac{d[Cu^I(t)]_{corr}}{dt} = -2k_{ox}[Cu^I(t)]^2_{corr} \quad \text{(S9)}$$

Since $[Cu^I(t)]_{corr}$ is the concentration of Cu^I that is oxidizable by O_2 as a function of time, Eq. (S9) can be integrated from 0 to *t*, and subsequently rearranged to yield:

$$Cu^I \text{ Fraction} = \frac{[Cu^I(t)]}{[Cu_{total}]} = \frac{1-[Cu^I(\infty)]/[Cu^I(0)]}{1+2k_{ox}([Cu^I(0)]-[Cu^I(\infty)])t} + \frac{[Cu^I(\infty)]}{[Cu^I(0)]} \quad \text{(S10)}$$

where k_{ox} and $[Cu^I(\infty)]$ are the fitted parameters. For each data series, $[Cu^I(\infty)]$ is set equal to the Cu^I fraction of the final time point, and non-linear least-squares regression was used to obtain the best-fit parameter of k_{ox} (listed in Table 3, main text).

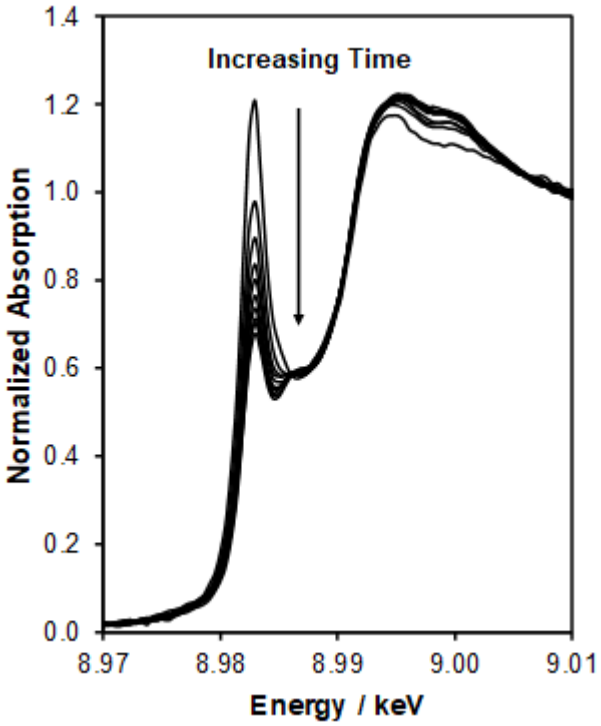

Figure S13. Time-resolved XANES spectra measured during the transient oxidation of Cu-CHA-0.078 (473 K, 10 kPa O_2) after treatment in 0.030 kPa NO and 0.030 kPa NH_3 at 473 K. A total of 40 spectra were collected in 20 second intervals. The first 10 spectra are plotted for clarity.

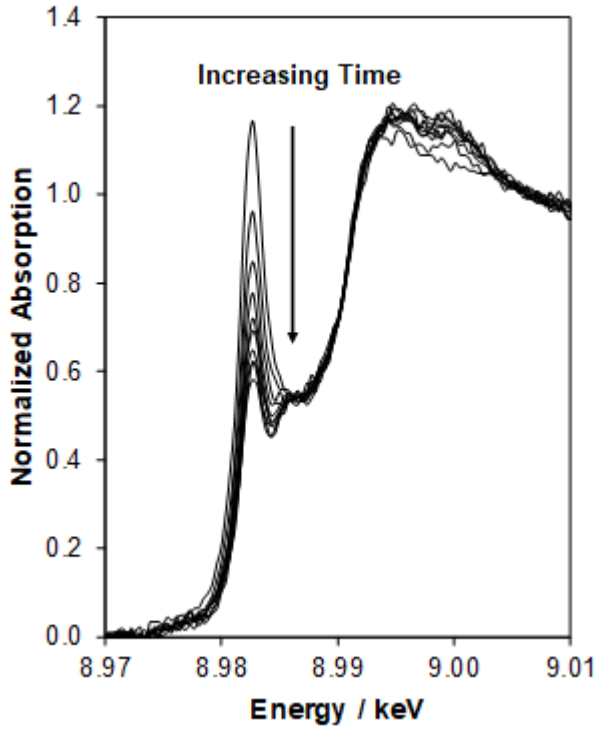

Figure S14. Time-resolved XANES spectra measured during the transient oxidation of Cu-CHA-0.10 (473 K, 10 kPa O_2) after treatment in 0.030 kPa NO and 0.030 kPa NH_3 at 473 K. A total of 40 spectra were collected in 20 second intervals. The first 10 spectra are plotted for clarity.

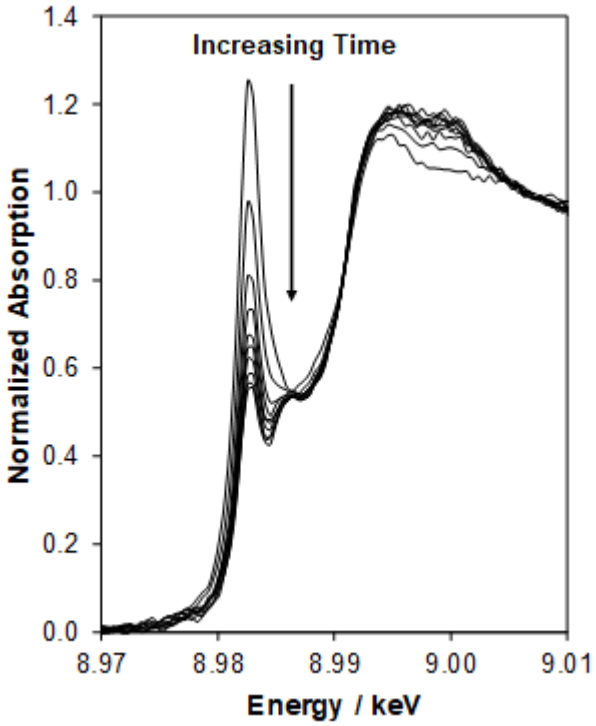

Figure S15. Time-resolved XANES spectra measured during the transient oxidation of Cu-CHA-0.17 (473 K, 10 kPa O_2) after treatment in 0.030 kPa NO and 0.030 kPa NH_3 at 473 K. A total of 40 spectra were collected in 14.5 second intervals. The first 10 spectra are plotted for clarity.

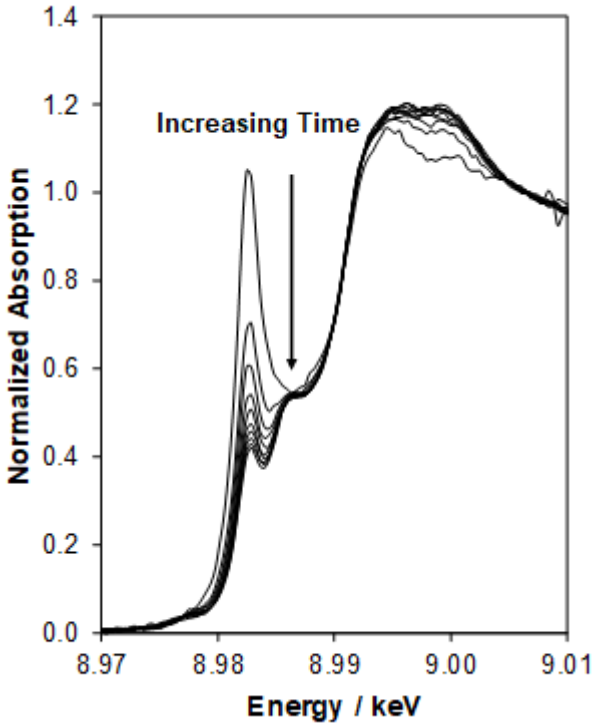

Figure S16. Time-resolved XANES spectra measured during the transient oxidation of Cu-CHA-0.23 (473 K, 10 kPa O_2) after treatment in 0.030 kPa NO and 0.030 kPa NH_3 at 473 K. A total of 30 spectra were collected in 21.5 second intervals. The first 10 spectra are plotted for clarity.

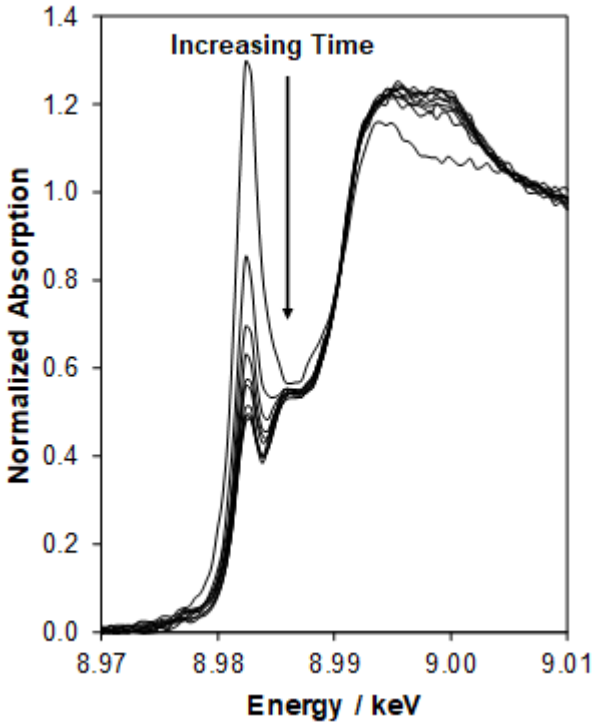

Figure S17. Time-resolved XANES spectra measured during the transient oxidation of Cu-CHA-0.29 (473 K, 10 kPa O_2) after treatment in 0.030 kPa NO and 0.030 kPa NH_3 at 473 K. A total of 39 spectra were collected in 14.5 second intervals. The first 10 spectra are plotted for clarity.

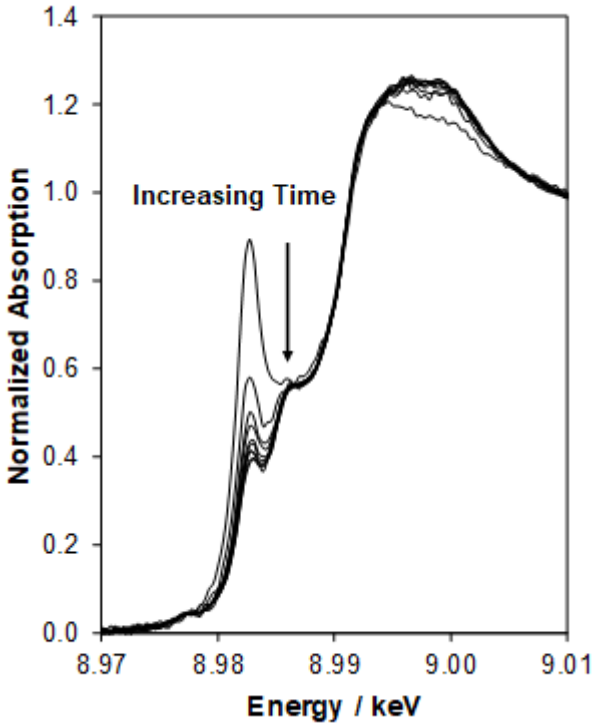

Figure S18. Time resolved XANES spectra measured during the transient oxidation of Cu-CHA-0.31 (473 K, 10 kPa O_2) after treatment in 0.030 kPa NO and 0.030 kPa NH_3 at 473 K. A total of 32 spectra were collected in 21.5 second intervals. The first 10 spectra are plotted for clarity.

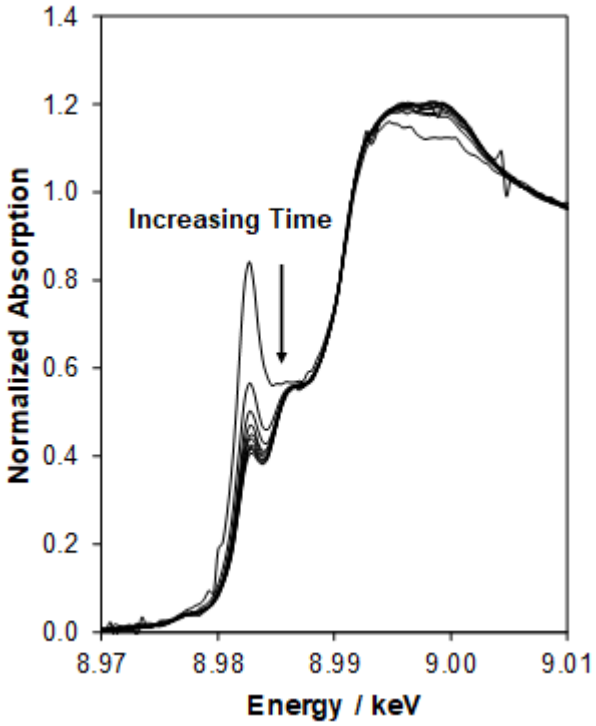

Figure S19. Time-resolved XANES spectra measured during the transient oxidation of Cu-CHA-0.35 (473 K, 10 kPa O_2) after treatment in 0.030 kPa NO and 0.030 kPa NH_3 at 473 K. A total of 30 spectra were collected in 21.5 second intervals. The first 10 spectra are plotted for clarity.

Section S.8. Transient NO+NH_3-assisted reduction of oxidized Cu-CHA-X samples: Models to fit rate data and corresponding XANES spectra

The transient decrease in Cu^{II} during reduction in NO and NH_3 can be described by a rate law that is first-order in Cu:

$$\frac{d[Cu^{II}(t)]}{dt} = -k_{red}[Cu^{II}(t)] \quad \text{(S11)}$$

In some samples studied, XANES spectra at the end of the transient NO+NH_3-assisted reduction experiments (Figs. S20-S24) showed small percentages (≤10%) of Cu^{II} that were not reduced, although we note that these values are within the uncertainty of the linear combination XANES fitting procedure. For the purposes of modeling the data in Figure 6 (main text), we define the fraction of Cu that are able to reduce as:

$$[Cu^{II}(t)]_{corr} = [Cu^{II}(t)] - [Cu^{II}(\infty)] \quad \text{(S12)}$$

$$\frac{d[Cu^{II}(t)]_{corr}}{dt} = -k_{red}[Cu^{II}(t)]_{corr} \quad \text{(S13)}$$

Integration of Eq. (S13) yields the following expression:

$$Cu^{II}\ \text{Fraction} = \frac{[Cu^{II}(t)]}{[Cu_{total}]} = \frac{[Cu_0^{II}]-[Cu_\infty^{II}]}{[Cu_{total}]} e^{-k_{red}t} + \frac{[Cu_\infty^{II}]}{[Cu_{total}]} \quad \text{(S14)}$$

Where k_{red} and $[Cu^{II}(\infty)]$ are fitted parameters. For each data series, $[Cu^{II}(\infty)]$ was set equal to the Cu^{II} fraction of the final time point, and non-linear least-squares regression was used to obtain the best-fit parameter of k_{red} (listed in Table 3, main text).

The transient reduction rate constants measured here were compared to a similar experiment reported in the literature by Liu et al. [8] using the following approximations. First, their reported initial rate of NO and NH_3 reduction (1.7 mmol NO g^{-1} h^{-1} at 0.05 kPa NO and 423 K) was converted to the units of our reduction rate constant:

$$1.7\ \frac{\text{mmol NO}}{\text{g h}} \times \frac{1\ \text{g cat}}{0.02\ \text{g Cu}} \times \frac{63.546\ \text{g Cu}}{\text{mol}} \times \frac{1\ \text{h}}{3600\ \text{s}} \times \frac{1\ \text{mol}}{1000\ \text{mmol}} = 0.0015\ \frac{\text{mol NO}}{\text{mol Cu s}} \quad \text{(S15)}$$

Next, the Arrhenius equation was applied to estimate this rate at 473 K, assuming an activation energy of 70 kJ/mol, which is consistent with reported apparent activation energies for low-temperature SCR in the reduction-limited regime [2,9]:

$$r_{NO,473K} = r_{NO,423K} \times e^{\frac{E_a}{R}\left[\frac{1}{423}-\frac{1}{473}\right]} = 0.012\ \frac{mol\ NO}{mol\ Cu\ s} \qquad \text{(S16)}$$

Finally, it was assumed that transient NO and NH_3 reduction is first-order in NO, and this rate was scaled by the ratio of NO pressures in the two experiments (3/5) to achieve the final estimate for the rate constant of 0.007 s^{-1}, which is quantitatively consistent with our measurement.

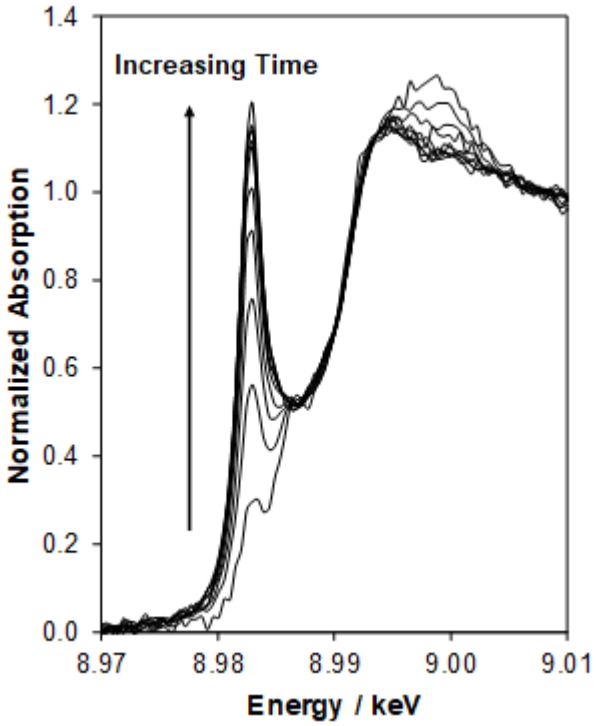

Figure S20. Time-resolved XANES spectra measured during the transient reduction of Cu-CHA-0.078 (473 K, 0.030 kPa NH_3, 0.030 kPa NO) after treatment in 20 kPa O_2 at 673 K. A total of 30 spectra were collected in 16.5 second intervals. The first 10 spectra are plotted for clarity.

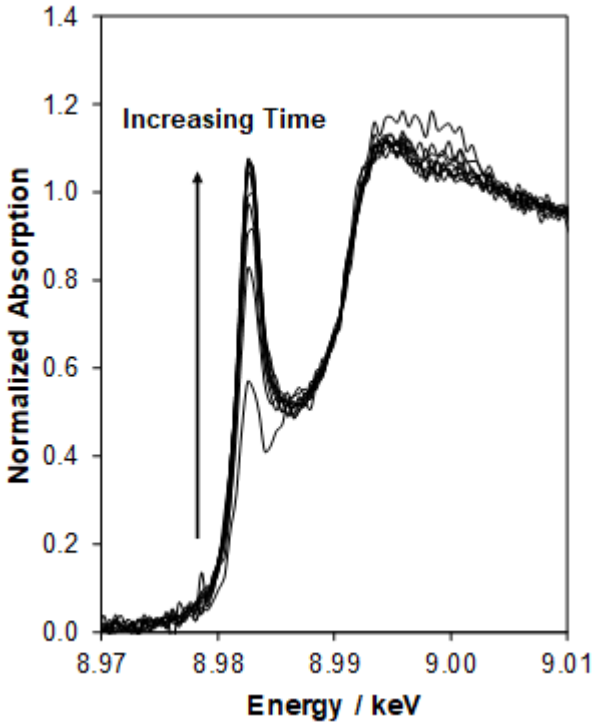

Figure S21. Time-resolved XANES spectra measured during the transient reduction of Cu-CHA-0.084 (473 K, 0.030 kPa NH_3, 0.030 kPa NO) after treatment in 20 kPa O_2 at 673 K. A total of 37 spectra were collected in 22.5 second intervals. The first 10 spectra are plotted for clarity.

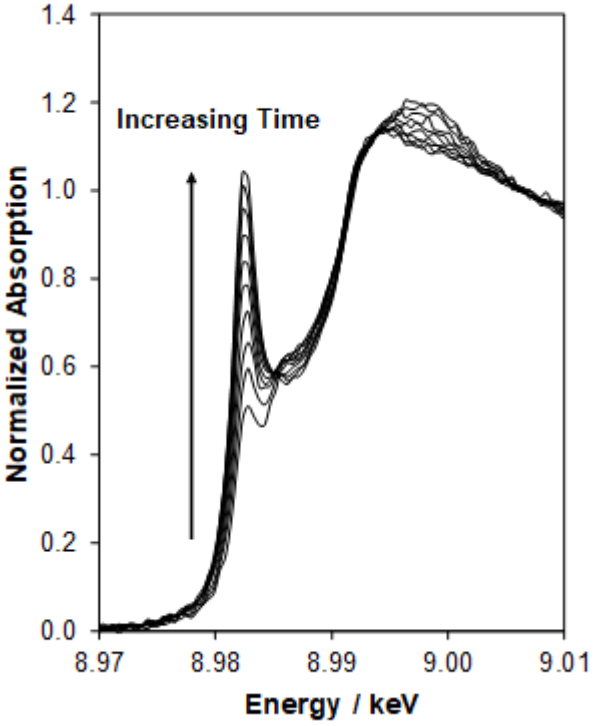

Figure S22. Time-resolved XANES spectra measured during the transient reduction of Cu-CHA-0.17 (473 K, 0.030 kPa NH_3, 0.030 kPa NO) after treatment in 20 kPa O_2 at 673 K. A total of 40 spectra were collected in 14.5 second intervals. The first 10 spectra are plotted for clarity.

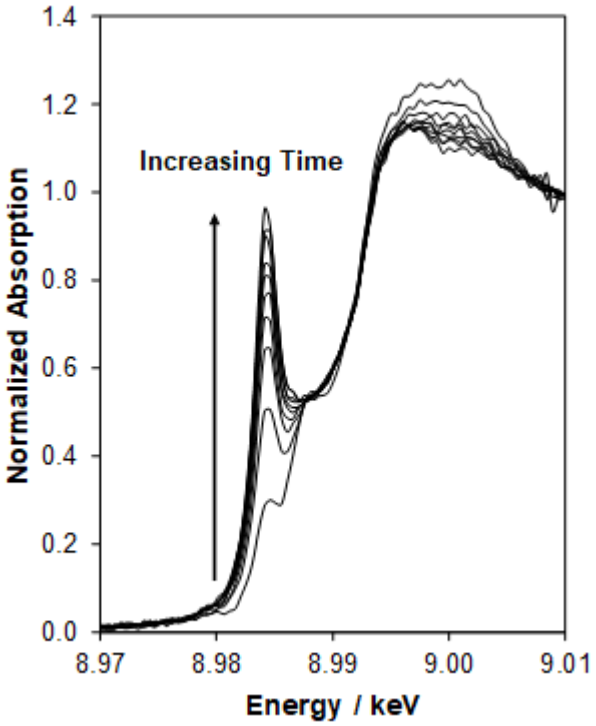

Figure S23. Time-resolved XANES spectra measured during the transient reduction of Cu-CHA-0.23 (473 K, 0.030 kPa NH_3, 0.030 kPa NO) after treatment in 20 kPa O_2 at 673 K. A total of 54 spectra were collected in 22.5 second intervals. The first 10 spectra are plotted for clarity.

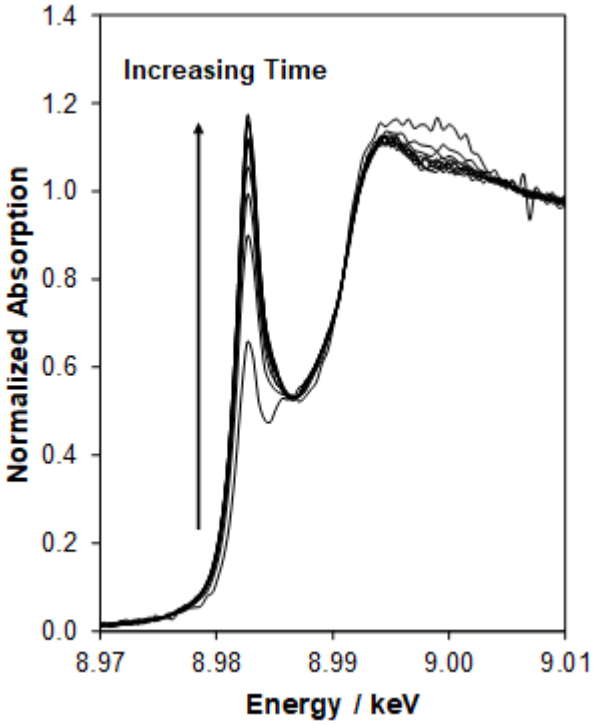

Figure S24. Time resolved XANES spectra measured during the transient reduction of Cu-CHA-0.35 (473 K, 0.030 kPa NH_3, 0.030 kPa NO) after treatment in 20 kPa O_2 at 673 K. A total of 21 spectra were collected in 22.5 second intervals. The first 10 spectra are plotted for clarity.

Section S.9. References

[1] C. Paolucci, A.A. Parekh, I. Khurana, J.R. Di Iorio, H. Li, J.D. Albarracin Caballero, A.J. Shih, T. Anggara, W.N. Delgass, J.T. Miller, F.H. Ribeiro, R. Gounder, W.F. Schneider, Catalysis in a Cage: Condition-Dependent Speciation and Dynamics of Exchanged Cu Cations in SSZ-13 Zeolites., J. Am. Chem. Soc. 138 (2016) 6028–48. https://doi.org/10.1021/jacs.6b02651.

[2] C. Paolucci, I. Khurana, A.A. Parekh, S. Li, A.J. Shih, H. Li, J.R.D. Iorio, J.D. Albarracin-Caballero, A. Yezerets, J.T. Miller, W.N. Delgass, F.H. Ribeiro, W.F. Schneider, R. Gounder, Dynamic multinuclear sites formed by mobilized copper ions in NOx selective catalytic reduction, Science. 357 (2017) 898–903. https://doi.org/10.1126/science.aan5630.

[3] H. Tsukahara, T. Ishida, M. Mayumi, Gas-Phase Oxidation of Nitric Oxide: Chemical Kinetics and Rate Constant, Nitric Oxide. 3 (1999) 191–198. https://doi.org/10.1006/niox.1999.0232.

[4] P.B. Weisz, C.D. Prater, Interpretation of Measurements in Experimental Catalysis, in: W.G. Frankenburg, V.I. Komarewsky, E.K. Rideal (Eds.), Adv. Catal., Academic Press, 1954: pp. 143–196. https://doi.org/10.1016/S0360-0564(08)60390-9.

[5] J.R. Di Iorio, C.T. Nimlos, R. Gounder, Introducing Catalytic Diversity into Single-Site Chabazite Zeolites of Fixed Composition via Synthetic Control of Active Site Proximity, ACS Catal. 7 (2017) 6663–6674. https://doi.org/10.1021/acscatal.7b01273.

[6] D.M. Ruthven, Z. Xu, Diffusion of oxygen and nitrogen in 5A zeolite crystals and commercial 5A pellets, Chem. Eng. Sci. 48 (1993) 3307–3312. https://doi.org/10.1016/0009-2509(93)80214-B.

[7] A.J. O'Malley, I. Hitchcock, M. Sarwar, I.P. Silverwood, S. Hindocha, C.R.A. Catlow, A.P.E. York, P.J. Collier, Ammonia mobility in chabazite: insight into the diffusion component of the NH3-SCR process, Phys. Chem. Chem. Phys. 18 (2016) 17159–17168. https://doi.org/10.1039/C6CP01160H.

[8] C. Liu, H. Kubota, T. Amada, K. Kon, T. Toyao, Z. Maeno, K. Ueda, J. Ohyama, A. Satsuma, T. Tanigawa, N. Tsunoji, T. Sano, K. Shimizu, In Situ Spectroscopic Studies on the Redox Cycle of NH3–SCR over Cu-CHA Zeolites, ChemCatChem. (n.d.). https://doi.org/10.1002/cctc.202000024.

[9] F. Gao, D. Mei, Y. Wang, J. Szanyi, C.H.F. Peden, Selective Catalytic Reduction over Cu/SSZ-13: Linking Homo- and Heterogeneous Catalysis, J. Am. Chem. Soc. 139 (2017) 4935–4942. https://doi.org/10.1021/jacs.7b01128.